Chemical Physics 515 (2018) 46–51

Contents lists available at ScienceDirect

Chemical Physics

journal homepage: www.elsevier.com/locate/chemphys

Floque Hamiltonian for incorporating electronic excitation by a laser pulse into simulations of non-adiabatic dynamics

Dmitry V. Makhov[a,b,*], Dmitrii V. Shalashilin[a]

[a] School of Chemistry, University of Leeds, Leeds LS2 9JT, United Kingdom
[b] School of Mathematics, University of Bristol, Bristol BS8 1TW, United Kingdom

A B S T R A C T

We present a simple way to incorporate a molecule-field interaction into non-adiabatic molecular dynamics. This makes possible integrated simulation of the photoexcitaion and the ensuing photodynamics, providing accurate initial conditions that are specific for the particular wave-length and duration of the laser pulse. The proposed approach is applied to simulate the dynamics of pyrrole photodissociation. The approach is particularly convenient for the use with *ab initio* Multiple Cloning approach, but the idea can be implemented in other quantum dynamics methods.

1. Introduction

Since the pioneering paper of Sobolewski and Domcke [1] that showed the existence of conical intersections in the decay channel of pyrrole, the mechanisms of its ultrafast photochemistry have been in the focus of numerous experimental [2–8] and theoretical [9–20] works. In recent years, the femtosecond experimental techniques have become particularly popular [5–7]. On the theoretical side, *ab initio* direct dynamics methods that can simulate quantum dynamics on the ultrafast time scale, such as *Ab initio* Multiple Spawning (AIMS) [21,22] and *Ab initio* Multiple Cloning (AIMC) [23,24] techniques, have been developed. For example, our AIMC simulations of pyrrole photodissociation [19,20] were able to reproduce correctly the main features of experimental total kinetic energy release (TKER) spectra and velocity map image (VMI) [7], and shed light on the reaction dynamics at the time scale of few hundreds of femtoseconds.

In theoretical simulations, Frank-Condon initial conditions are usually used, when the lowest vibrational state of the ground electronic state is simply “lifted up” to the excited electronic state. This choice of initial conditions disregards the dynamics that occurs during the excitation pulse, which is not always a very good approximation, given that the time scale of the pulse (~ 50 fsec) is not much shorter than that of the simulated non-adiabatic dynamics (~ 100–200 fsec). It also does not take into account the coordinate dependence of transition dipoles, which can be important especially in the case of symmetry-prohibited transitions. The most rigorous way to generate proper initial conditions for the photodynamics initiated by a short laser pulse would be to simulate the very process of electronic excitation together with non-adiabatic dynamics for the particular frequency, duration and shape of the laser pulse. In order to do so, the interaction of the molecule with the laser field must be incorporated into the Hamiltonian.

Direct dynamics simulation of the excitation was implemented in a number of different ways in framework of AIMS algorithm [25–28]. The AIMS method, however, was initially designed for treating non-adiabatic dynamics at conical intersections where the coupling between states is extremely localized, while coupling with electric field is not localised. As a result, simulation of electronic excitation in AIMS would require lot of spawning in order to keep electronic states coupled for a sufficiently long time. In particular, the resent XFAIMS (eXternal Field *Ab Initio* Multiple Spawning) method [27] spawns a new trajectory twice per optical period, each time the absolute value of the electric field reaches its maximum. Test simulations for LiH excitation show that the results provided by XFAIMS are in close agreement with numerically exact quantum dynamics. As an example, the method was used to simulate the excitation of H_2CSO molecules by 0.85 fs and 2.54 fs laser pulses and to study the effect of nuclear motion on population transfer of during photoexcitation.

In this work, we report the implementation of simultaneous simulations of laser excitation and non-adiabatic dynamics in the Multiple Cloning framework. AIMC approach is very well suited for such simulations as it is based on Ehrenfest coherent states, which provide a continuous coupling between electronic states removing the necessity of extensive spawning. We treat laser field as a Floquet quantum oscillator coupled with the molecule through the electric dipole operator. Floque Hamiltonian was used before with AIMS approach [25,26] but it was replaces by direct periodic perturbation in a recent XFAIMS method, which has advantage for ultra-short pulses that exhibit a significant uncertainty in frequency. On the other hand, the use of Floque

* Corresponding author at: School of Chemistry, University of Leeds, Leeds LS2 9JT, United Kingdom.
E-mail address: d.makhov@leeds.ac.uk (D.V. Makhov).

https://doi.org/10.1016/j.chemphys.2018.07.048

Available online 11 August 2018

Hamiltonian is extremely convenient for the simulation of excitation by longer pulses in the AIMC framework, as the coupling with laser field can be handled with almost no extra efforts in exactly the same way as non-adiabatic coupling in the standard AIMC algorithm. Only one additional potential energy surface $V_0 + \hbar\omega$ should be introduced representing the electronic ground state shifted up by one quantum of the field.

2. Theory

The interaction of the molecular system with external laser field is usually described by adding a periodic perturbation $\mathbf{E}\cdot\mathbf{d}\cos(\omega t)$ to a molecule Hamiltonian, where the amplitude of the field $\mathbf{E}(t)$ depends on time slowly. However, fast oscillations caused by $\cos(\omega t)$ in this additional term make interaction with the field in the Hamiltonian extremely inconvenient for numerical simulations. On the other hand, it is well known that the dynamics in a quantum system with potential energy surfaces $V_0, V_1, \ldots, V_k$ acted upon by a periodic perturbation of frequency ω is equivalent to the dynamics driven by the time independent Hamiltonian with additional states $V_0 \pm n\hbar\omega$, $V_1 \pm n\hbar\omega$, …, $V_k \pm n\hbar\omega$, which are the original states shifted by integer numbers of the optical field quanta $\hbar\omega$. This is known as Floquet Hamiltonian [29] or the ladder of quasienergies [30].

Floquet theory, which effectively quantises the field, provides easy and straightforward way to treat the molecule-field interaction. In this work, we are interested only in the linear absorption and do not consider processes involving more than one photon. In this situation, we can take into account only zero and one photon quantum states of the external field, which we denote as $|0\rangle$ and $|1\rangle$. Moreover, as only the electronic ground sate is populated initially, we do not need to include any excited states of the molecule for state $|1\rangle$ of the field. Thus, we can incorporate the process of photoexcitation into our simulations by adding just one more state, namely Floquet state with the energy $V_0 + \hbar\omega$, to our AIMC dynamics! Below, we will refer this Floquet state as $\widetilde{S}_0$, while electronic states for state $|0\rangle$ of the field will be referred as S_0, S_1, S_2 *etc*.

Within the framework of AIMC method, the total wave-function $|\Psi$ is represented in a trajectory-guided basis $|\psi_n\rangle$:

$$|\Psi\rangle = \sum_n c_n(t)|\psi_n(t)\rangle \tag{1}$$

In an original AIMC ansatz, the basis functions $|\psi_n\rangle$ are composed of the nuclear and electronic parts. Here we add a third part $|f\rangle$ representing a quantum state of the external field:

$$|\psi_n(t)\rangle = |\chi_n(t)\rangle \sum_{I,f} a_{If}^{(n)}(t)|\phi_I\rangle|f\rangle, \tag{2}$$

where $|\phi_I\rangle$ are the electronic eigenstates of the molecule, and $|f\rangle$ representing the field is either $|0\rangle$ or $|1\rangle$. As it was mentioned above, we include here only electronic ground state $|\phi_0\rangle$ of the molecule for state $|1\rangle$, and all electronic states for state $|0\rangle$ of the field.

As before, a nuclear part $|\chi_n(t)\rangle$ of each basis function is a Gaussian Coherent State moving along Ehrenfest trajectory:

$$\chi_n(t) = \left(\frac{2\alpha}{\pi}\right)^{N_{dof}/4} \exp\left(-\alpha(\mathbf{R}-\overline{\mathbf{R}}_n(t))^2 + \frac{i\overline{\mathbf{P}}_n(t)\cdot(\mathbf{R}-\overline{\mathbf{R}}_n(t))}{\hbar} + \frac{i}{\hbar}\gamma_n(t)\right) \tag{3}$$

with $\overline{\mathbf{R}}_\mathbf{n}$ and $\overline{\mathbf{P}}_\mathbf{n}(t)$ representing the coordinate and momentum of the center of nth Gaussian, and phase $\gamma_n(t)$ propagated as

$$\dot{\gamma}_n = \frac{\overline{\mathbf{P}}_n\overline{\mathbf{R}}_n}{2}. \tag{4}$$

There are two different approaches to the choice of the electronic basis functions $|\phi_I\rangle$ in Eq. (2). Traditionally, adiabatic eigenfunctions $|\phi_I\rangle = |\phi_I(\mathbf{r};\mathbf{R})\rangle$ are used; in this case the non-adiabatic coupling comes from the kinetic energy operator $\left(-\frac{\hbar^2}{2}\nabla_\mathbf{R}\mathbf{M}^{-1}\nabla_\mathbf{R}\right)$ acting on $|\phi_I(\mathbf{r};\mathbf{R})\rangle$ due to its parametric dependence on $\mathbf{R}$. Alternatively, electronic part of each function $|\psi_n(t)\rangle$ can be represented using its own set of diabatic functions $|\phi_I^{(n)}\rangle$ that coincide with adiabatic eigenfunctions in the centre of the Gaussian $|\phi_I^{(n)}\rangle = |\phi_I(\mathbf{r};\overline{\mathbf{R}}_n(t))\rangle$. This approach is known as time-dependent diabatic (TDD) [24,31] basis or moving crude adiabatic (MCA) [32] basis. The non-adiabatic coupling in TDD basis comes from the time dependence of basis functions $|\phi_I^{(n)}\rangle$ due to the motion of the Gaussian.

Calculations in TDD basis are slightly more complicated than those in an adiabatic basis, as the overlaps between electronic functions $|\phi_I^{(n)}\rangle$ for different Gaussians need now to be calculated and taken into account in propagation of amplitudes $c_n(t)$. However, TDD approach has a number of important advantages: 1) it treats correctly the interaction between basis functions around very sharp crossings, where adiabatic approach fails; 2) it naturally accounts for the geometric phase, the effect of which (although negligible for pyrrole [33]) can modify non-adiabatic dynamics in profound ways [34]; 3) the non-adiabatic coupling does not have a second order term in TDD basis. The second-order coupling is difficult to integrate due to divergence of its integrals with Gaussians [35], and it is usually neglected in non-adiabatic dynamics simulations; nevertheless, it still can be important in some cases [36].

It can be shown [23] that both adiabatic and TDD approaches lead to the same set of equations when adiabatic eigenstates $\phi_I(\mathbf{r};\mathbf{R})$ change smoothly with $\mathbf{R}$, i.e., when the overlaps between electronic functions $|\phi_I^{(n)}\rangle$ for all pairs of Gaussians with non-zero nuclear overlap can be assumed to be Kronecker's δ_{IJ} and when the second-order non-adiabatic coupling can be ignored. This approximation usually works well for small molecules, such as pyrrole, while for large conjugated polymers and dendrimers, where adiabatic electronic states can change instantly at trivial unavoided crossings [37] between spatially separated non-interacting electronic states, the accurate TDD approach should be used.

For the sake of brevity and in order to be consistent with our previous works on pyrrole [19,20], we are also using the above approximation (i.e., assume smooth change of adiabatic eigenfunctions) in the present work. It should be noticed that the choice of adiabatic or TDD basis is not essential here, and the equations below can be easily modified to be used in either of them.

The propagation of Ehrenfest amplitudes $a_{If}^{(n)}$ for each trajectory is described by the same equation as in the standard AIMC

$$\dot{a}_{If}^{(n)} = -\frac{i}{\hbar}\sum_{J,g} H_{IJfg}^{(n)} a_{Jg}^{(n)}, \tag{5}$$

but the matrix elements of Hamiltonian $H_{IJfg}^{(n)}$ now include, in addition to the non-adiabatic coupling, the interaction with laser field:

$$H_{IJfg}^{(n)} = \begin{cases} V_I(\overline{\mathbf{R}}_n), & I = J, \quad f = g = |0\rangle \\ -i\hbar\overline{\mathbf{P}}_n\mathbf{M}^{-1}\mathbf{C}_{IJ}(\overline{\mathbf{R}}_n), & I \neq J, \quad f = g = |0\rangle \\ V_0(\overline{\mathbf{R}}_n) + \hbar\omega, & I = J = 0, \quad f = g = |1\rangle \\ \mathbf{E}\cdot\mathbf{d}_I(\overline{\mathbf{R}}_n), & J = 0, \quad f \neq g \\ \mathbf{E}\cdot\mathbf{d}_J(\overline{\mathbf{R}}_n), & I = 0, \quad f \neq g \end{cases} \tag{6}$$

Here $\mathbf{C}_{IJ} = \langle\phi_I(\mathbf{r};\mathbf{R})|\nabla_\mathbf{R}\phi_J(\mathbf{r};\mathbf{R})\rangle$ are non-adiabatic coupling vectors, $\mathbf{d}_I = \langle\phi_0|\,\hat{\mathbf{d}}\,|\phi_I\rangle$ are transition dipoles, V_I are potential energies, and $\mathbf{E}$ is the amplitude of laser field. First two lines in Eq. (6) represent a usual non-adiabatic Hamiltonian. Third line is a potential energy term for state $|\phi_0\rangle|1\rangle$, which is shifted by $\hbar\omega$ with respect to the ground state $|\phi_0\rangle|0\rangle$ reflecting the energy of a photon. Fourth and fifth lines represent the coupling between state $|\phi_0\rangle|1\rangle$ and the excited states of the molecule, which is responsible for electronic excitation associated with the absorption of a photon. Matrix elements $H_{IJfg}^{(n)}$ are calculated "on the fly" in the course of dynamics, with potential energies, non-adiabatic coupling vectors, and transitional dipoles given by the electronic structure code. Thus, Hamiltonian (6) takes into account the coordinate dependence of transition dipoles $\mathbf{d}_I$ providing the way for correct description of electron-vibrational coupling during the process of photoexcitation.

The coupling with the field is no longer oscillatory.

Because we consider only a linear case here, a weak external field is not affecting the motion of Gaussians, and they are guided by standard Ehrenfest force:

$$\mathbf{F} = -\sum_{I,f} |a_{If}|^2 \nabla E_I + \sum_{I\neq J,f} a^*_{If} a_{Jf} \mathbf{C}_{IJ}(V_I - V_J). \tag{7}$$

Eqs. (4)–(7) form a complete set for the propagation of the basis.

The evolution of the total wave-function can be found by substituting ansatz (1) into the time dependent Schrodinger Equation:

$$\sum_n \langle \psi_m(t)|\psi_n(t)\rangle \dot{c}_n(t) = -\frac{i}{\hbar}\sum_n \left(H_{mn} - i\hbar\left\langle \psi_m(t)\left|\frac{d}{dt}\right|\psi_n(t)\right\rangle\right)c_n(t) \tag{8}$$

The form of Eq. (6) is exactly the same as in the standard AIMC but the matrix elements H_{mn} now include additional terms:

$$\begin{aligned} H_{mn} = &\left\langle \chi_m \left| -\frac{\hbar^2}{2}\nabla_{\mathbf{R}}\mathbf{M}^{-1}\nabla_{\mathbf{R}}\right|\chi_n\right\rangle + \sum_I (a^{(m)}_{I0})^* a^{(n)}_{I0}\langle \chi_m | V_I | \chi_n\rangle \\ &+ (a^{(m)}_{01})^* a^{(n)}_{01}\langle \chi_m | V_0 + \hbar\omega | \chi_n\rangle\langle \chi_m | \chi_n\rangle\hbar\omega \\ &-\hbar^2\sum_{I\neq J}(a^{(m)}_{I0})^* a^{(n)}_{J0}\langle \chi_m | \mathbf{C}_{IJ}\mathbf{M}^{-1}\nabla | \chi_n\rangle \\ &+ \sum_I [(a^{(m)}_{01})^* a^{(n)}_{I0} + (a^{(m)}_{I0})^* a^{(n)}_{01}]\langle \chi_m | \mathbf{d}_I\cdot\mathbf{E} | \chi_n\rangle \end{aligned} \tag{9}$$

First terms here is a kinetic energy; second and third terms are potential energies for states $|0\rangle$ and $|1\rangle$ of the field respectively (we take into account only ground state in the latter case). The forth term is a usual non-adiabatic coupling, and the fifth term is the coupling between the molecule and the field. While the matrix element of the kinetic energy can be calculated analytically, for other matrix elements, we use a simple approximation proposed in our previous work [23]:

$$\begin{aligned} \langle \chi_m | V_I(\mathbf{R}) | \chi_n\rangle = &\langle \chi_m | \chi_n\rangle\left(\frac{V_I(\overline{\mathbf{R}}_m) + V_I(\overline{\mathbf{R}}_n)}{2}\right) \\ &+ \frac{\langle \chi_m | (\mathbf{R}-\overline{\mathbf{R}}_m)|\chi_n\rangle \nabla V_I(\overline{\mathbf{R}}_m) + \langle \chi_m | (\mathbf{R}-\overline{\mathbf{R}}_n)|\chi_n\rangle \nabla V_I(\overline{\mathbf{R}}_n)}{2}, \end{aligned} \tag{10}$$

$$\langle \chi_m | \mathbf{C}_{IJ}(\mathbf{R})\mathbf{M}^{-1}\nabla | \chi_n\rangle = \frac{i}{2h}\langle \chi_m | \chi_n\rangle(\overline{\mathbf{P}}_m\mathbf{M}^{-1}\mathbf{C}_{IJ}(\overline{\mathbf{R}}_m) + \overline{\mathbf{P}}_n\mathbf{M}^{-1}\mathbf{C}_{IJ}(\overline{\mathbf{R}}_n)), \tag{11}$$

$$\langle \chi_m | \mathbf{d}_{IJ}\cdot\mathbf{E} | \chi_n\rangle = \frac{1}{2}\langle \chi_m | \chi_n\rangle(\mathbf{d}_{IJ}(\overline{\mathbf{R}}_m) + \mathbf{d}_{IJ}(\overline{\mathbf{R}}_n))\cdot\mathbf{E} \tag{12}$$

The term $\left\langle \psi_m(t)\left|\frac{d}{dt}\right|\psi_n(t)\right\rangle$ in Eq. (8), which reflects the time dependence of the basis, can be expressed as:

$$\begin{aligned} \left\langle \psi_m(t)\left|\frac{d}{dt}\psi_n(t)\right.\right\rangle = &\left\langle \chi_m \left| \frac{d}{dt}\chi_n\right.\right\rangle \sum_{I,f}(a^{(m)}_{If})^* a^{(n)}_{If} \\ &+ \langle \chi_m | \chi_n\rangle \sum_{I,f}(a^{(m)}_{If})^* \frac{d}{dt}a^{(n)}_{If}, \end{aligned} \tag{13}$$

where

$$\left\langle \chi_m \left| \frac{d}{dt}\chi_n\right.\right\rangle = \dot{\overline{\mathbf{R}}}_n\left\langle \chi_m \left| \frac{d}{d\overline{\mathbf{R}}_n}\right|\chi_n\right\rangle + \dot{\overline{\mathbf{P}}}_n\left\langle \chi_m \left| \frac{d}{d\overline{\mathbf{P}}_n}\right|\chi_n\right\rangle + \frac{i}{\hbar}\dot{\gamma}_n\langle \chi_m | \chi_n\rangle. \tag{14}$$

Due to approximation (10)-(12), all matrix elements in (9) are calculated from the electronic structure data used for the propagation of the basis. This allows us to calculate amplitudes $c_n(t)$ in post-processing using the saved trajectory data, as in a standard AIMC algorithm. As the electronic structure is the most expensive part of *on the fly* calculations, quantum coupling between the configurations in our approach comes a practically no additional computational cost.

3. Cloning

Cloning is the key element of AIMC dynamics that distinguishes it from the Multi-Configurational Ehrenfest (MCE) [38,39] method. When cloning is applied, a single Ehrenfest configuration is replaces by two new configurations, one of which has nonzero amplitudes for only one electronic state, while the second clone contains contributions of all other electronic states:

$$|\psi'_n\rangle = |\chi_n\rangle\left(\frac{a^{(n)}_{If}}{|a^{(n)}_{If}|}\times|\phi_I\rangle|f\rangle + \sum_{(J,g)\neq(I,f)} 0\times|\phi_J\rangle|g\rangle\right) \tag{15}$$

and

$$|\psi'_{n'}\rangle = |\chi_n\rangle\left(0\times|\phi_I\rangle|f\rangle + \frac{1}{\sqrt{1-|a^{(n)}_{If}|^2}}\sum_{(J,g)\neq(I,f)}|\phi_J\rangle|g\rangle\right). \tag{16}$$

The amplitudes of the two new configurations are adjusted in such a way that their total contribution to the whole wave function (1) remains the same as the contribution of the original configuration:

$$c'_n = c_n\,|a^{(n)}_{If}|, \quad c'_{n'} = c_n\sqrt{1-|a^{(n)}_{If}|^2}\,. \tag{17}$$

In a standard AIMC, cloning is used to allow the bifurcation of the wave-function at conical intersections. Thus, it is applied when breaking force

$$\mathbf{F}^{(\mathrm{br})} = |a_{If}|^2\left(\nabla V_I - \sum_{J,g}|a_{Jg}|^2\nabla V_J\right), \tag{18}$$

which is the force pulling $|\phi_I\rangle|f\rangle$ state away from the remaining states, exceeds a threshold for at least one state, while non-adiabatic coupling is low at the same time. Thus, trajectory basis functions are usually cloned just after passing a intersection if, due to the partial population transfer, two electronic states with different potential energy gradients have significant Ehrenfest amplitudes.

The above cloning conditions are also applied in the present work for the non-adiabatic part of the dynamics. However, they a not appropriate for cloning out the excited states from the initial trajectory. The dynamics now starts from Floquet state $\widetilde{S}_0$ and, while photoexcitation populates other states, these populations are still very low in the linear case considered in this paper. Nevertheless, these states need to be cloned out with reasonably short time intervals: without cloning, the Ehrenfest configuration would simply follow the trajectory on the state $\widetilde{S}_0$. It is cloning that initiates the excited states trajectories which describe the subsequent non-adiabatic dynamics. Thus, for the initial Floquet state trajectory, the cloning is performed every time when $\widetilde{S}_0$ state energy term crosses one of the exited state energy terms, as illustrated in Fig. 1. Cloning in these crossing points ensures that the additional classical energy of exited state trajectories corresponds to the energy of photon. This approach provides sufficiently frequent cloning if the laser frequency ω is chosen in a high absorption region, i.e. close to one of the transition energies of the molecule.

It should be noticed that although absolute amplitudes of the exited state trajectories generated as a result of cloning are low, their absolute values do not have much importance here: they simply reflect a share of exited molecules in the ensemble and, as such, are determined by the intensity of laser pulse. What is important are the relative amplitudes of different excited state trajectories and the relative amplitudes of different states for each of them.

4. Algorithm

The algorithm that we use for modelling photoexcitation is illustrated in Fig. 2. We start from the Floquet state $\widetilde{S}_0$ (i.e., from the ground state $|\phi_0\rangle$ of the molecule and state $|1\rangle$ of the external field), and run a set of trajectories with initial coordinates and momenta randomly

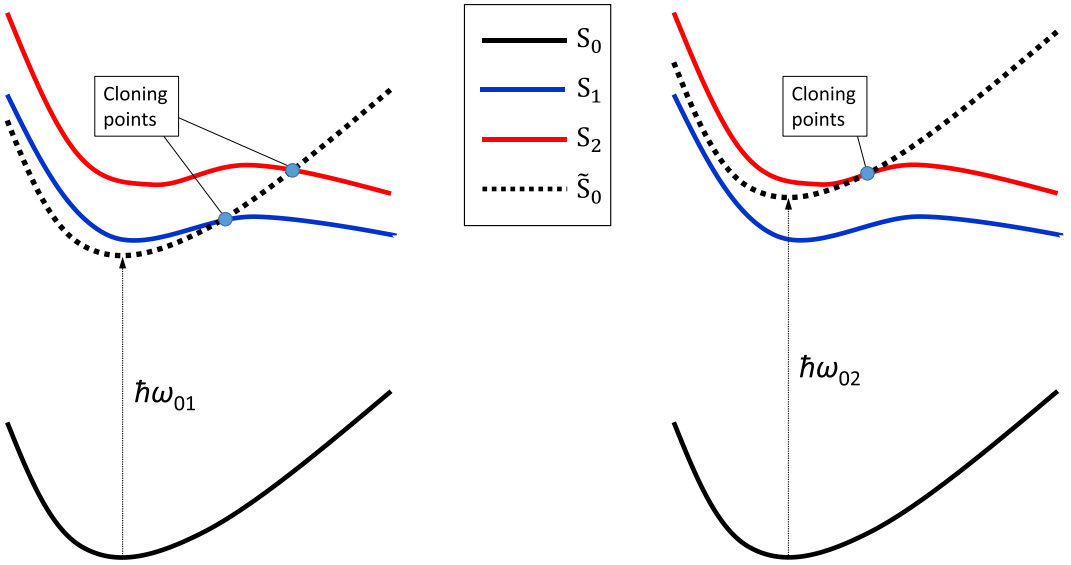

Fig. 1. The sketch of pyrrole energy terms used in the simulation of photoexcitation dynamics with laser pulse frequencies approximately corresponding to the energies of $S_0 \rightarrow S_1$ (left) and $S_0 \rightarrow S_2$ (right) transitions. The difference between these two cases is in the position of Floquet state $\widetilde{S}_0$, which is a ground state shifted by $\hbar\omega$. Cloning is applied when Floquet state $\widetilde{S}_0$ term crosses one of the excited state terms. (Here we show just few crossing points, while their number in reality is large for multi-dimensional motion.)

generated, as usual, according to Wigner distribution. This initial trajectories are run only for the duration of laser pulse, as state $\widetilde{S}_0$ does not participate in non-adiabatic dynamics. Instead it is coupled to the excited states S_1, S_2, *etc* through molecule-field interaction, and this provides the growth of excited states populations over the duration of the laser pulse. The use of Ehrenfest approach ensures that the electronic states remain coupled for a long time helping to treat correctly the oscillation of the population flux due to transition energy mismatch during photoexcitation.

Every time the potential energy term for $\widetilde{S}_0$ state crosses the excited state term (i.e. when transition energy is exactly equal to the frequency of the field), the cloning is applied. These cloning events launch a swarm of trajectories on the excited states S_1, S_2, *etc* for non-adiabatic dynamics initiated by the photoexcitation. Those, in turn, can undergo more clonings while passing through the regions of high non-adiabatic coupling, now initiated by strong breaking force (18) as in the usual AIMC dynamics.

When all trajectories are calculated, we use them to propagate basis sets, which are composed of Gaussian coherent states. Solving Eq. (8) provides amplitudes $c_n(t)$ for the representation (1) of the total wavefunction $|\Psi\rangle$.

5. Computational details and results

In order to test the proposed approach, the calculations were run to simulate the process of pyrrole photoexcitation by a 50 fs laser pulse and its subsequent dissociation. As before [19,20], trajectories were calculated using AIMS-MOLPRO [40] computational package modified to incorporate Ehrenfest dynamics, the cloning thresholds were taken as 5×10^{-6} a.u for the breaking acceleration of Eq. (18) and 2×10^{-3} a.u. for the norm of non-adiabatic coupling vector, and complete active space self-consistent field (CASSCF) method at SA4-CAS(8,7)/cc-pVDZ level was used for the electronic structure. The width of Gaussian functions α was taken as 4.7, 22.7 and 19.0 Bohr^{-2} for hydrogen, carbon nitrogen atoms respectively, as suggested in Ref. [41].

Calculations were run for two pulse frequencies ω corresponding to approximate energies of $S_0 \rightarrow S_1$ and $S_0 \rightarrow S_2$ transitions of pyrrole. It is well known that CASSCF method somewhat overestimate transition energies, so the frequencies were taken $\hbar\omega_{01} = 0.168$ Hartree for $S_0 \rightarrow S_1$ and $\hbar\omega_{02} = 0.192$ Hartree for $S_0 \rightarrow S_2$ transition to match our electronic structure data, not the experimental pyrrole spectrum.

A bunch of 200 trajectories starting from $\widetilde{S}_0$ state and randomly generated according to Wigner distribution coordinates and momenta was run for 50 fs – the duration of the laser pulse. For $\omega = \omega_{01}$, 1094 $\widetilde{S}_0$–S_1 crossings points and 30 $\widetilde{S}_0$–S_2 crossings points were identified, and the excited state trajectories initiated at these points undergo 229 more clonings during non-adiabatic dynamics, making 1353 branches in total. For $\omega = \omega_{02}$, the numbers of $\widetilde{S}_0$–S_1 and $\widetilde{S}_0$–S_2 crossing points were 15 and 1551 respectively, and the number of further cloning events was 187, making 1753 branches in total.

Fig. 3 presents the time-dependences of electronic state populations for two pulse frequencies. The results were averaged over all initial trajectories and 100 random orientations of the molecule with respect to the laser field. The population of $\widetilde{S}_0$ state is not shown here for an obvious reason: it reflects only the share of the molecules that remained unexcited, which is close to 1 in the linear regime. As a result, the populations in Fig. 3 are not normalized, and the fact that the total population in part (B) is larger than in part (A) simply means the higher rate of absorption at ω_{02} frequency.

One can see that the processes of photoexcitation and nonradiative decay occur on the same time scale. For $\omega = \omega_{01}$, the growth of S_1 population due to photoexcitation is immediately followed by its relaxation to a ground state. State S_2 is practically not involved here, as a molecule does not have enough energy to go there. For $\omega = \omega_{02}$, the excitation to S_2 is also followed by quick non-adiabatic relaxation, first to S_1 and then to S_0 state. The population of S_2 states reaches its maximum at 45 fs; by the end of the pulse, the relaxation dominates over the photoexcitation making S_2 populations go down.

Fig. 4 shows calculated total kinetic energy release (TKER) spectrum for pyrrole photodissociation. To plot this spectrum, each trajectory leading to dissociation was ascribed a weight based on the final amplitudes c_n of appropriate basis functions. Then, the spectrum was smoothed by replacing delta-functions with Gaussian functions ($\sigma = 200$ cm^{-1}). The spectra for both values of ω were normalized to simplify the comparison. The experimental [7] TKER spectra of pyrrole

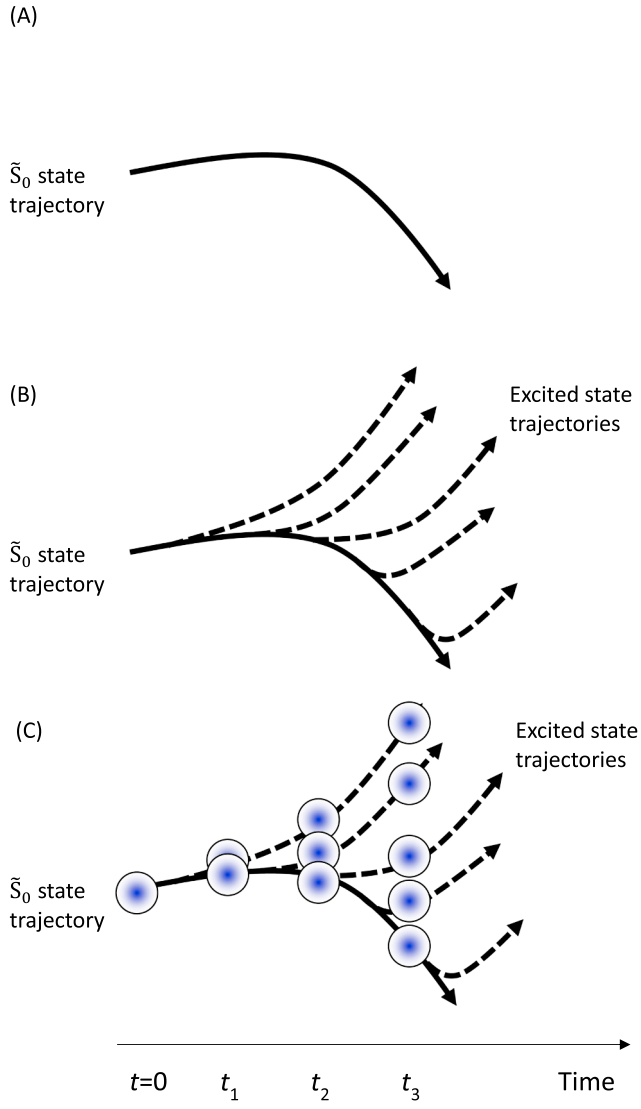

Fig. 2. The sketch illustrating our algorithm for modelling the photoexcitation. (A) Initial ground $\tilde{S}_0$ state trajectory. (B) Cloning out excited states at crossing points. (C) The motion and growing of the basis used to solve time-dependent Schrodinger Equation.

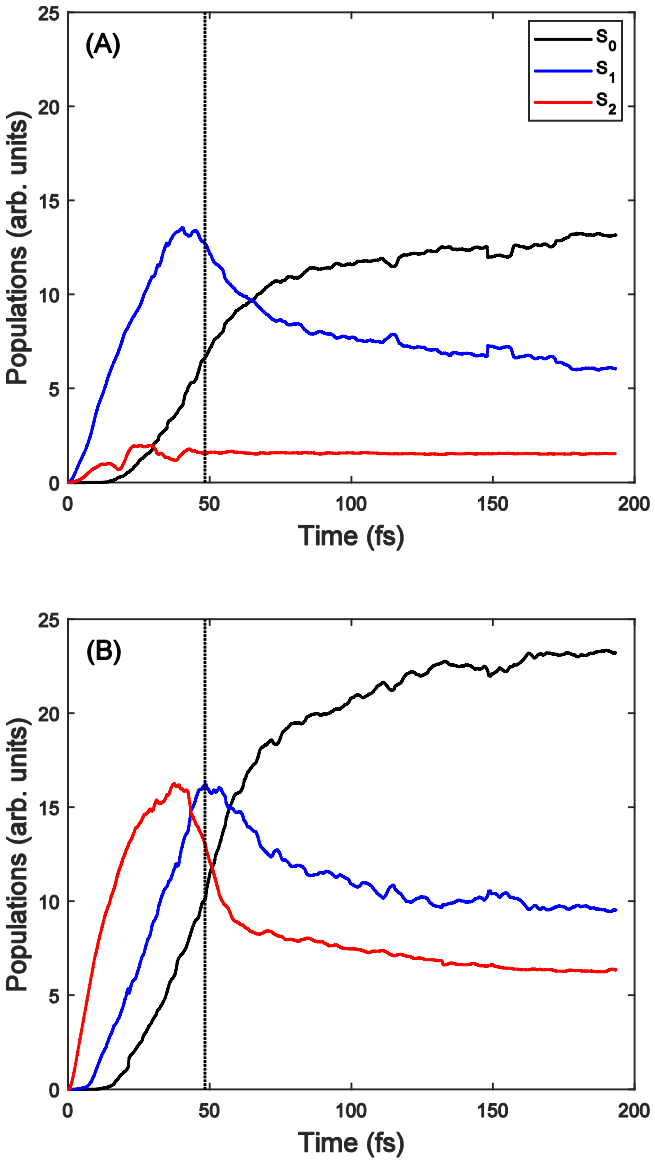

Fig. 3. Electronic state populations as a function of time. Laser pulse frequencies approximately correspond to the transition energies of S_1 (A) and S_2 (B) states. The duration of laser pulse is shown by a dot line. Excitation and dynamics occur simultaneously.

for 250 nm and 238 nm wave-length are shown in the insert. One can see that the calculated spectrum for higher ω is wider, which reproduces the experimental trend. On the other hand, the calculations do not show the shift of the position of the main peak as the frequency increases: the excess of the pumped energy remains in form of the electronic excitation of the radical, which exhibit larger relative population of the exited states in the higher-frequency case (see Fig. 3). Also, the absolute values of the energies are about 1.5 times on average higher than in experiment. This can be ascribed to the inaccuracy of CASSCF electronic structure method, which, in particular, overestimate transition energies due to the lack of dynamic electron correlations. Nevertheless, our calculations illustrate the importance of treating the excitation and non-adiabatic dynamics simultaneously and show that the proposed approach can capture experimentally observed dependence of the dynamics on excitation pulse frequency and duration.

6. Conclusion

Non-adiabatic dynamics simulations usually apply very primitive initial conditions where ground vibrational wave packet is simply lifted to one of the excited states. In this work, we have proposed the way to avoid this approximation by modelling the process of photoexciteation together with the dynamics. In our algorithm, the laser field is treated using a quantum approach; this allows us to incorporate field-molecule interaction into a standard AIMC dynamics by simply adding just one new quantum state that is a ground state shifted by $\hbar\omega$ and coupled to excited states through transitions dipoles.

In order to test the method, we have used it to simulate the process of the photodissociation of pyrrole. The dependence of calculated TKER spectrum on the laser pulse wave-lengths is in a qualitative agreement with the experiment, although more calculations for different molecular systems are needed in order to evaluate the accuracy and efficiency of the proposed approach.

The proposed idea is very versatile and can be applied not only together with AIMC but with any technique (e.g., vMCG or MCTDH) used for the simulations of the ultrafast photodynamics.

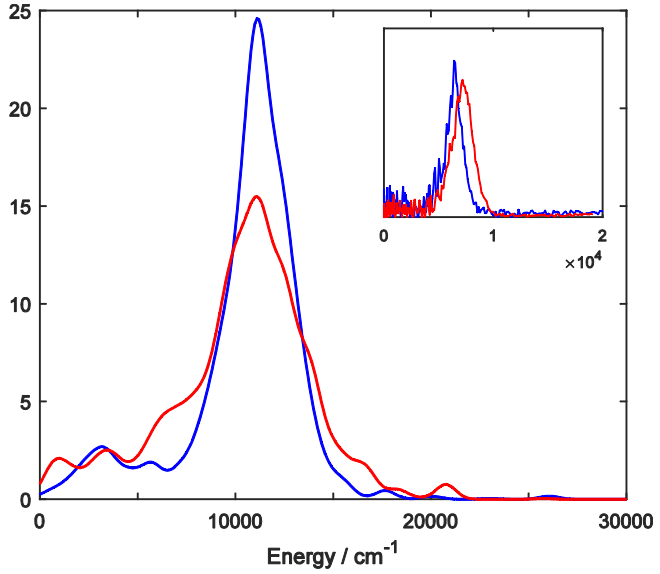

Fig. 4. Calculated TKER spectrum for pyrrole photodissociation by 50 fs laser pulse. The wave-lengths approximately correspond to the transition energies of S_1 (blue) and S_2 (red) states. An experimental TKER spectra of pyrrole for 250 nm and 238 nm wave-lengths from Ref. [7] are shown in the insert. (For interpretation of the references to colour in this figure legend, the reader is referred to the web version of this article.)

Acknowledgements

This work has been supported by EPSRC through grants EP/P021123/1 and EP/N007549/1, and by the Leverhulme trust through grant RPG-2015-190. We would also like to thank Basile Curchod for useful discussions of XEAIMS and the use of Floque Hamiltonian within AIMS method.

References

[1] A.L. Sobolewski, W. Domcke, Chem. Phys. 259 (2000) 181.
[2] B. Cronin, A.L. Devine, M.G.D. Nix, M.N.R. Ashfold, PCCP 8 (2006) 3440.
[3] L. Rubio-Lago, D. Zaouris, Y. Sakellariou, D. Sofikitis, T.N. Kitsopoulos, F. Wang, X. Yang, B. Cronin, A.L. Devine, G.A. King, M.G.D. Nix, M.N.R. Ashfold, S.S. Xantheas, J. Chem. Phys. 127 (2007) 064306.
[4] J. Wei, J. Riedel, A. Kuczmann, F. Renth, F. Temps, Faraday Discuss. 127 (2004) 267.
[5] H. Lippert, H.H. Ritze, I.V. Hertel, W. Radloff, ChemPhysChem 5 (2004) 1423.
[6] R. Montero, Á.P. Conde, V. Ovejas, M. Fernández-Fernández, F. Castaño, J.R.V.D. Aldana, A. Longarte, J. Chem. Phys. 137 (2012).
[7] G.M. Roberts, C.A. Williams, H. Yu, A.S. Chatterley, J.D. Young, S. Ullrich, V.G. Stavros, Faraday Discuss. 163 (2013) 95.
[8] C.T. Middleton, K. de La Harpe, C. Su, Y.K. Law, C.E. Crespo-Hernandez, B. Kohler, Annu. Rev. Phys. Chem. 60 (2009) 217.
[9] A.L. Sobolewski, W. Domcke, C. Dedonder-Lardeux, C. Jouvet, PCCP 4 (2002) 1093.
[10] M. Barbatti, J. Pittner, M. Pederzoli, U. Werner, R. Mitric, V. Bonacic-Koutecky, H. Lischka, Chem. Phys. 375 (2010) 26.
[11] Z. Lan, A. Dupays, V. Vallet, S. Mahapatra, W. Domcke, J. Photochem. Photobiol. Chem. 190 (2007) 177.
[12] S. Mahapatra, Acc. Chem. Res. 42 (2009) 1004.
[13] V. Vallet, Z. Lan, S. Mahapatra, A.L. Sobolewski, W. Domcke, Faraday Discuss. 127 (2004) 283.
[14] V. Vallet, Z.G. Lan, S. Mahapatra, A.L. Sobolewski, W. Domcke, J. Chem. Phys. 123 (2005) 144307.
[15] M. Barbatti, M. Vazdar, A.J.A. Aquino, M. Eckert-Maksić, H. Lischka, J. Chem. Phys. 125 (2006) 164323.
[16] B. Sellner, M. Barbatti, H. Lischka, J. Chem. Phys. 131 (2009) 024312.
[17] M. Vazdar, M. Eckert-Maksić, M. Barbatti, H. Lischka, Mol. Phys. 107 (2009) 845.
[18] K. Saita, M.G.D. Nix, D.V. Shalashilin, PCCP 15 (2013) 16227.
[19] D.V. Makhov, K. Saita, T.J. Martinez, D.V. Shalashilin, PCCP 17 (2015) 3316.
[20] D.V. Makhov, T.J. Martinez, D.V. Shalashilin, Faraday Discuss. 194 (2016) 81.
[21] M. Ben-Nun, T.J. Martínez, Advances in Chemical Physics, John Wiley & Sons Inc:, 2002, p. 439.
[22] T.J. Martinez, M. BenNun, G. Ashkenazi, J. Chem. Phys. 104 (1996) 2847.
[23] D.V. Makhov, W.J. Glover, T.J. Martinez, D.V. Shalashilin, J. Chem. Phys. 141 (2014) 054110.
[24] D.V. Makhov, C. Symonds, S. Fernandez-Alberti, D.V. Shalashilin, Chem. Phys. 493 (2017) 200.
[25] J. Kim, H. Tao, J.L. White, V.S. Petrović, T.J. Martinez, P.H. Bucksbaum, J. Phys. Chem. A 116 (2012) 2758.
[26] J. Kim, H. Tao, T.J. Martinez, P. Bucksbaum, J. Phys. B: At. Mol. Opt. Phys. 48 (2015) 164003.
[27] B. Mignolet, B.F.E. Curchod, T.J. Martínez, J. Chem. Phys. 145 (2016) 191104.
[28] B. Mignolet, B.F.E. Curchod, J. Chem. Phys. 148 (2018) 134110.
[29] J.H. Shirley, Phys. Rev. 138 (1965) B979.
[30] A.I. Baz', I.A.B. Zel'dovich, A.M. Perelomov, Scattering, Reactions and Decay in Nonrelativistic Quantum Mechanics: (Rasseyanie, Reaktsii i Raspady V Nerelyativistskoi Kvantovoi Mekhanike), Israel Program for Scientific Translations, 1969.
[31] S. Fernandez-Alberti, D.V. Makhov, S. Tretiak, D.V. Shalashilin, PCCP 18 (2016) 10028.
[32] L. Joubert-Doriol, J. Sivasubramanium, I.G. Ryabinkin, A.F. Izmaylov, J. Phys. Chem. Lett. 8 (2017) 452.
[33] S.C. Althorpe, T. Stecher, F. Bouakline, J. Chem. Phys. 129 (2008) 214117.
[34] I.G. Ryabinkin, L. Joubert-Doriol, A.F. Izmaylov, Acc. Chem. Res. 50 (2017) 1785.
[35] G.A. Meek, B.G. Levine, J. Chem. Phys. 144 (2016) 184109.
[36] I.G. Ryabinkin, L. Joubert-Doriol, A.F. Izmaylov, J. Chem. Phys. 140 (2014) 214116.
[37] S. Fernandez-Alberti, A.E. Roitberg, T. Nelson, S. Tretiak, J. Chem. Phys. 137 (2012) 014512.
[38] D.V. Shalashilin, J. Chem. Phys. 132 (2010) 244111.
[39] K. Saita, D.V. Shalashilin, J. Chem. Phys. 137 (2012) 22A506.
[40] B.G. Levine, J.D. Coe, A.M. Virshup, T.J. Martinez, Chem. Phys. 347 (2008) 3.
[41] A.L. Thompson, C. Punwong, T. Martinez, J. Chem. Phys. 370 (2010) 70.